Analytical Characterization of SOA-Based Optical Pulse Delay Discriminator

Malin Premaratne, *Senior Member, IEEE*, and Arthur James Lowery, *Senior Member, IEEE*

***Abstract*—Semiconductor optical amplifier (SOA)-based optical timing extraction and clock-recovery schemes offer compact size, low operating power, and added possibility for integration into an all-optical circuitry. In this paper, we analyze a device that could measure the relative delay between counterpropagating pulses incident on an SOA. Unlike previous designs based on differential photodiodes, our optical pulse delay discriminator (OPDD) uses the voltage difference between two contacts on the SOA. We therefore eliminate the two photodiodes and two optical couplers, making integration far easier. After giving a qualitative description of the operation of the proposed design, we carry out a comprehensive analytical analysis of the operation of the device performance. At each stage, we demonstrate the accuracy of the derived approximate formulas. An analytical expression for the transient response of OPDD shows it to be exponential with a time constant set by the carrier-recovery lifetime. We show that it is possible to reliably measure the incident delay between counterpropagating, periodic pulse trains by measuring the mean value (or low-pass-filtered value) of the induced voltage difference. Our analysis shows the OPDD has excellent linearity.**

***Index Terms*—Clock recovery, integrated optoelectronic circuits, photonic circuits, semiconductor optical amplifiers (SOAs).**

I. Introduction

THE comparison of phase and timing of modulated optical waveforms is critical to the design of all-optical clocks using phase-locked loops [1]. Optical timing extraction and clock recovery [2]–[5] play a significant role in applications such as demultiplexing [6] and 3R (reamplification, reshaping, and retiming) regeneration [7], [8]. Semiconductor optical amplifier (SOA)-based schemes ([2], [4], [7]) have attracted much interest because of their compact size, low operating power, and added possibility for integration into an all-optical circuitry. The operation principles rely on nonlinear gain saturation and cross-gain modulation. [7], [9], [10].

Short picosecond pulse propagation in SOAs has been widely studied for applications in optical communications systems [9], [10]. Even though the main motive for such studies was to investigate the amplification properties of SOAs, it is clear that SOAs play a major role in optical signal processing [11], [12]. The effectiveness of SOAs in all-optical integrated circuitry results from their high-gain coefficients and low saturation power [9], [10].

In 2002, Awad *et al.* [7] demonstrated that by simply comparing the time-averaged output powers at the ends of an SOA, it is possible to measure the relative delay between pulses. Awad *et al.* [7] used couplers and photodiodes to detect the powers of the counterpropagating waves exiting the SOA as shown in Fig. 1. The photocurrents are fed into a low-speed differential amplifier to obtain a signal proportional to the relative timing of the pulses.

In this paper, we use the detection properties of an SOA's contact voltage [15], [16] to measure the relative delay between two pulse trains. This again relies on cross-gain modulation, but in our device, the longitudinal dependence of the gain also becomes important. The difference in the contact voltages at the ends of the SOA indicates which pulse traverses the SOA first. This is because the first pulse will receive the most gain, substantially reducing the carrier density by gain saturation at the end from which it exits. The second pulse will receive less gain, and so will reduce the carrier density at the end from which it exits. The contact voltages are dependent on the local carrier density, and therefore indicate which pulse was first. Furthermore, because the gain recovers between the pulses, closely spaced pulses will cause a greater voltage difference.

This scheme was proposed and tested numerically in [4]; this paper develops expressions to confirm the simulations. These expressions give fresh insight into the operation of the optical pulse delay discriminator (OPDD). In Section II, we derive approximate expressions for the longitudinal carrier-density profile evolution and the related optical-gain response for three different cases of interest: Section II-A derives the response to a single pulse; Section II-B covers two identical counterpropagating pulses; and Section II-C extends the derivation to two counterpropagating periodic pulse trains. In each of these cases, we demonstrate the accuracy and validity of the derivations using numerical calculations. In Section III, we introduce quantitative expressions to compare the OPDD scheme and Awad's scheme. In Section III-A, we derive explicit expressions for the transient response and show that it is exponential with a time constant given by the carrier-recovery lifetime of SOAs. In Section III-B, we demonstrate the linearity of the OPDD and derive an approximate analytical expression to characterize the linear region. Based on these observations, we give guidelines for designing OPDDs in Section IV. We conclude this paper in Section V.

II. Approximate Analytical Characterization of Response of SOA to Short Pulses

In this section, we develop approximate analytical results to characterize the response of SOA when it is fed by a single short optical pulse, two identical counterpropagating pulses, and two

Manuscript received March 1, 2005; revised April 6, 2005.

The authors are with the Advanced Computing and Simulation Laboratory (AXL), Department of Electrical and Computer Systems Engineering, Monash University, Clayton, Victoria 3800, Australia. (e-mail: malin@eng.monash.edu.au; arthur.lowery@eng.monash.edu.au).

Digital Object Identifier 10.1109/JLT.2005.853142

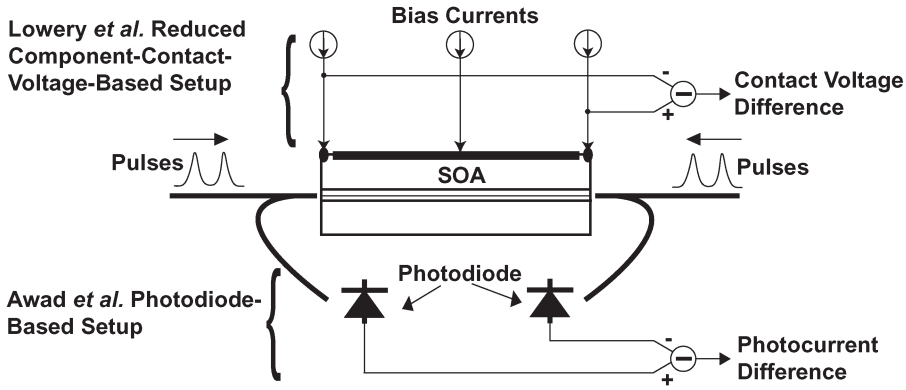

Fig. 1. Schematic diagram of the proposed pulse delay discriminator based on Lowery *et al.* [4] and the photocurrent-difference-based pulse discriminator of Awad *et al.* [7].

counterpropagating identical optical pulse trains. To make the system analytically tractable, we limit our analysis to a three-section device with very short end contacts, subject to pulses significantly narrower than the carrier-recovery lifetime.

A. Response to a Single Short Pulse

Suppose $H_{T_w}(t)$ is the intensity profile of an optical pulse with arbitrary shape but with a full-width at half-maximum (FWHM) of T_w and energy E_g. The latter assumption implies

$$E_g = A\int_{-\infty}^{+\infty} H_{T_w}(t)\mathrm{d}t \tag{1}$$

where A is the cross-sectional area of the SOA active region. We also assume that the carrier lifetime τ_e of the semiconductor medium is much greater than the FWHM of the optical pulse (i.e., $\tau_e \gg T_w$). The dynamic response of the SOA is given by [9], [13]

$$\frac{\partial}{\partial z}I(z,t) + \frac{1}{v_g}\frac{\partial}{\partial t}I(z,t) = g(z,t)I(z,t) - \alpha I(z,t) \tag{2}$$

$$\frac{\partial}{\partial t}N(z,t) = \wp(z) - \frac{N(z,t)}{\tau_e} - g(z,t)\frac{\lambda I(z,t)}{hc} \tag{3}$$

where t is time, z is distance along the SOA measured from the left facet, $I(z,t)$ is the intensity of the optical signal along the SOA, $N(z,t)$ is the carrier density along the SOA, α is the loss coefficient, Γ is the mode confinement factor, a is the differential gain coefficient, $g(z,t) = \Gamma a(N(z,t) - N_0)$, $\wp(z)$ is the current-injection density along the SOA, λ is the mean operating wavelength, c is the speed of light in vacuum, and h is the Plank's constant. To make subsequent analysis easier, we change our analysis reference frame to a moving coordinate system that moves with the forward-propagating pulse

$$\xi = z; \quad \tau = t - \frac{z}{v_g}. \tag{4}$$

These transformations give the following two differential operators for time and spatial partial derivatives

$$\frac{\partial}{\partial z} = \frac{\partial}{\partial \xi} - \frac{1}{v_g}\frac{\partial}{\partial \tau}; \quad \frac{\partial}{\partial t} = \frac{\partial}{\partial \tau}. \tag{5}$$

Substitution of (4) and (5) into (2) and (3) result in the following coordinate-transformed equations:

$$\frac{\partial}{\partial \xi}I(\xi,\tau) = g(\xi,\tau)I(\xi,\tau) - \alpha I(\xi,\tau) \tag{6}$$

$$\frac{\partial}{\partial \tau}N(\xi,\tau) = \wp(\xi) - \frac{N(\xi,\tau)}{\tau_e} - g(\xi,\tau)\frac{\lambda I(\xi,\tau)}{hc}. \tag{7}$$

To solve these equations when an intense short pulse is input to the SOA, we use the approach suggested by Siegman [14]. In his analysis of two-level amplifying systems, he used the assumption that the stimulated-emission-induced carrier depletion due to a short pulse (i.e., a pulse with FWHM pulsewidth much smaller than carrier lifetime) can be considered instantaneous. Just after the stimulated emission-induced carrier depletion, carriers will replenish themselves to the initial steady-state population through carrier injection, with a carrier-recovery lifetime τ. Applying this idea to an SOA, during the stimulated emission process, we derive from (7)

$$\frac{\partial}{\partial \tau}g(\xi,\tau) = -g(\xi,\tau)\frac{\Gamma\lambda a I(\xi,\tau)}{hc}. \tag{8}$$

Similar to the analysis of SOAs by Agrawal *et al.* [9], we try to construct a differential equation for the modal gain evolution along the amplifier. However, unlike the analysis in [9], we do not assume that the attenuation coefficient of an SOA is negligible. Therefore, our analysis is more general than previous results.

We can solve (6) to get the following exact solution:

$$I(\xi,\tau) = H_{T_w}(\tau)G(\xi,\tau) \tag{9}$$

where the total gain $G(\xi,\tau)$ along the amplifier is given by

$$G(\xi,\tau) = \exp\left(-\alpha\xi + \int_0^{\xi} g(\xi,\tau)\mathrm{d}\xi\right). \tag{10}$$

It is easy show from (10) that

$$\frac{1}{G(\xi,\tau)}\frac{\partial}{\partial\tau}G(\xi,\tau)=\frac{\partial}{\partial\tau}\int_0^{\xi}g(\xi,\tau)\mathrm{d}\xi. \tag{11}$$

We now integrate (8) with respect to ξ and substitute (11) to get

$$\frac{1}{G(\xi,\tau)}\frac{\partial}{\partial\tau}G(\xi,\tau)=-\frac{\Gamma\lambda a}{hc}\int_0^{\xi}g(\xi,\tau)I(\xi,\tau)\mathrm{d}\xi \tag{12}$$

after substituting (6) and (9) into (12), we get

$$\frac{\partial}{\partial\tau}\ln\left(G(\xi,\tau)\right)=-\frac{\Gamma\lambda a}{hc}H_{T_w}(\tau)\left(G(\xi,\tau)-1\right)-\frac{\Gamma\lambda a}{hc}\alpha\int_0^{\xi}I(\xi,\tau)\mathrm{d}\xi. \tag{13}$$

To evaluate the integral of the intensity along the SOA [see last term in (13)], momentarily we make the assumption (which will be relaxed later) that the differential gain is uniform along the SOA. This amounts to assuming that there exists a uniform gain coefficient $\bar{g}$ such that $G(\xi,\tau)\approx\exp(\bar{g}\xi-\alpha\xi)$. Therefore, using (9) we get

$$\int_0^{\xi}I(\xi,\tau)\mathrm{d}\xi\approx\frac{H_{T_w}(\tau)}{\bar{g}-\alpha}\left(G(\xi,\tau)-1\right). \tag{14}$$

Substituting (14) into (13), we get

$$\frac{\partial}{\partial\tau}\ln\left(G(\xi,\tau)\right)=-\frac{\Gamma\lambda a\bar{g}H_{T_w}(\tau)}{hc(\bar{g}-\alpha)}\left(G(\xi,\tau)-1\right). \tag{15}$$

After some algebraic manipulations, (15) becomes

$$\frac{\partial}{\partial\tau}\ln\left(\frac{G(\xi,\tau)}{G(\xi,\tau)-1}\right)=\frac{\Gamma\lambda a\bar{g}}{hc(\bar{g}-\alpha)}H_{T_w}(\tau) \tag{16}$$

performing integration with respect to τ and labeling gain just before pulse arrival as G_{init} and just after its influence on stimulated emission as G_{final}, we get

$$G_{\mathrm{final}}(\xi)=\frac{G_{\mathrm{init}}(\xi)}{\mathcal{G}_{\mathrm{init}}+G_{\mathrm{init}}(\xi)(1-\mathcal{G}_{\mathrm{init}})} \tag{17}$$

where we used following definition for $\mathcal{G}_{\mathrm{init}}$:

$$\mathcal{G}_{\mathrm{init}}=\exp\left(-\frac{\Gamma\lambda a\bar{g}E_g}{hc(\bar{g}-\alpha)A}\right). \tag{18}$$

Our main interest is to calculate the carrier density $N(\xi,\tau)$ along the SOA. From (10), we write the carrier-density distribution due to G_{final} as

$$\int_0^{\xi}N_{\mathrm{final}}(\xi)\mathrm{d}\xi=\frac{1}{\Gamma a}\ln\left(G_{\mathrm{final}}(\xi)\right)+\frac{\alpha}{\Gamma a}\xi+N_0\xi. \tag{19}$$

Differentiating (19) with respect to ξ and using (17), the depleted carrier density $N_{\mathrm{final}}(\xi)$ corresponding to $G_{\mathrm{final}}(\xi)$ can be written as

$$N_{\mathrm{final}}(\xi)\approx N_{\mathrm{init}}(\xi)-\frac{\left(N_{\mathrm{init}}(\xi)-N_0-\frac{\alpha}{\Gamma a}\right)\left(1-\mathcal{G}_{\mathrm{init}}\right)}{1-\mathcal{G}_{\mathrm{init}}+\frac{\mathcal{G}_{\mathrm{init}}}{G_{\mathrm{init}}(\xi)}} \tag{20}$$

where $N_{\mathrm{init}}(\xi)$ is the initial carrier density along the SOA before the arrival of the optical pulse.

Now, we switch back to the laboratory coordinate system for convenience. It is interesting to note that because $\xi=z$, (20) is invariant in this original coordinate system. Referring back to our reasoning at the beginning of this section, once the carrier depletion has taken place, carriers in the SOA will replenish by injection, at a rate governed by the carrier-recovery lifetime. Thus, from (3) we get

$$\frac{\partial}{\partial t}N(z,t)=\wp(z)-\frac{N(z,t)}{\tau_e}. \tag{21}$$

Solving this equation with the initial conditions $N(z,0)=N_{\mathrm{final}}(z)$ gives

$$N(z,t)=\tau_e\wp(z)+N_{\mathrm{final}}(z)\exp\left(-\frac{t}{\tau_e}\right)-\tau_e\wp(z)\exp\left(-\frac{t}{\tau_e}\right). \tag{22}$$

This shows that the depleted carrier density replenishes with a time constant τ_e [the first two terms in the right-hand side of (22)]. Also of interest is the evolution of modal gain given in (10). Substituting (22) into (10), we get

$$G(z,t)=\exp\left(\Gamma a\tau_e\int_0^{z}\wp(z)\mathrm{d}z\left(1-\exp\left(-\frac{t}{\tau_e}\right)\right)\right)\times\exp\left(-\alpha z+\Gamma a\int_0^{z}N_{\mathrm{final}}\mathrm{d}z\exp\left(-\frac{t}{\tau_e}\right)-\Gamma aN_0z\right). \tag{23}$$

This equation can be written in the following compact form using the instantaneously depleted gain G_{final}

$$G(z,t)=G_{\mathrm{ref}}(z)\left(\frac{G_{\mathrm{final}}(z)}{G_{\mathrm{ref}}(z)}\right)^{\exp\left(\frac{-t}{\tau_e}\right)} \tag{24}$$

where

$$G_{\mathrm{ref}}(z)=\exp\left(\Gamma a\left(\tau_e\int_0^{z}\wp(z)\mathrm{d}z-N_0z\right)\right). \tag{25}$$

To demonstrate the accuracy of the results derived so far, we use numerical simulations with the parameter values given in Table I. The numerical solutions in this and subsequent sections were calculated by directly numerically integrating the coupled (2) and (3) in MATLAB. Fig. 2 shows the carrier density N against position z at elapsed times of a) 0.0, b) 100.0 ps, and

TABLE I
PARAMETERS USED IN SIMULATIONS

SOA Length (L)	378.0×10^{-6} m
Active Region Width (w)	2.5×10^{-6} m
Active Region Thickness (d)	0.2×10^{-6} m
Waveguide Group Effective Index (n_g)	3.7
Loss Coefficient (α)	3000.0 m^{-1}
Carrier Recombination Coefficient (τ_e)	300.0×10^{-12} s
Carrier Injection Rate ($\wp$)	1.0567×10^{34} $\mathrm{s}^{-1}\mathrm{m}^{-3}$
Confinement Factor (Γ)	0.3
Material Gain Coefficient (a)	2.5×10^{-20} m^2
Transparency Carrier Density (N_0)	1.5×10^{24} m^{-3}
Nominal Wavelength (λ)	1552.52×10^{-9} m
Photodiode Responsivity (R)	1.0 AW^{-1}
Heterostructure Ideality Factor (η)	2.0

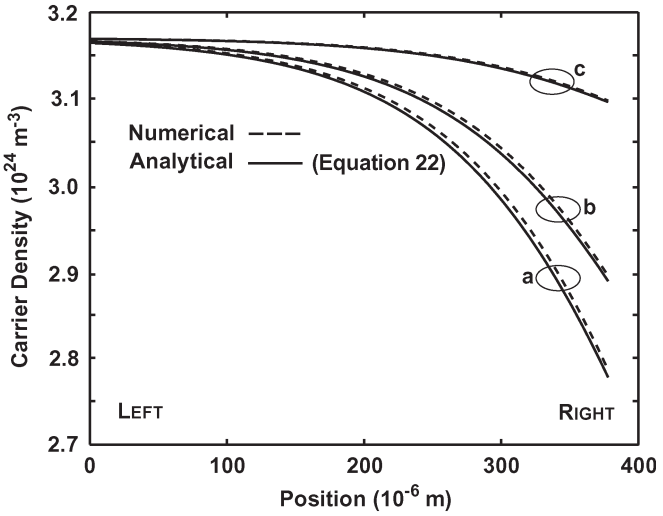

Fig. 2. Carrier density N against SOA position z: a) 0.0; b) 100.0; and c) 500.0 ps after pulse exit.

c) 500.0 ps, after a Gaussian pulse with 5.0-ps FWHM and 25.0-fJ energy has passed completely through the SOA. The dashed lines show the numerical simulation results, and the solid lines show the analytical solution of (22). Fig. 2 clearly shows that (22) is a very good approximation for representing dynamic carrier-density profile.

B. Response to Two Counterpropagating Identical Pulses

Consider two counterpropagating pulses with identical pulse profiles, both similar to the pulse considered in the previous section. Suppose the first pulse enters SOA from the left and, after τ seconds, the second pulse enters SOA from the right as shown in Fig. 3. We also assume that before the arrival of the first pulse, the SOA is in its steady state with carrier-density and gain profiles (see Fig. 3), as follows:

$$N_{\mathrm{init},1}(z) = \tau_e \wp(z) \tag{26}$$

$$G_{\mathrm{init},1}(z) = \exp\left(-\alpha z + \Gamma a \int_0^z (\tau_e \wp(z) - N_0)\,\mathrm{d}z\right). \tag{27}$$

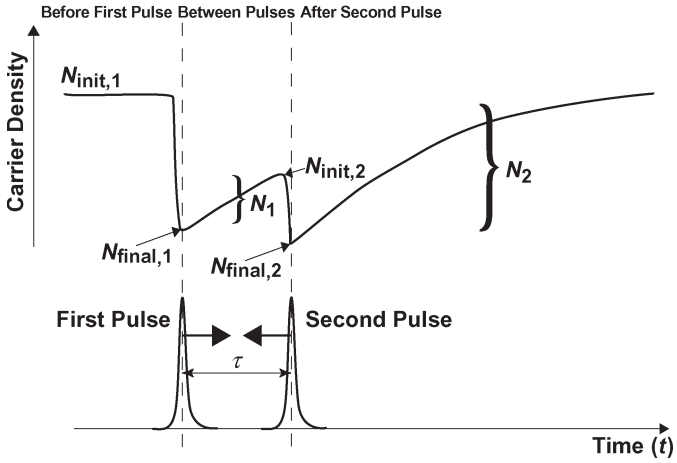

Fig. 3. Carrier-density evolution response (at an arbitrary position along the SOA) against time for two counterpropagating identical pulses with relative delay τ.

When the first pulse enters from the left, the carrier density evolves as (22), so

$$N_1(z,t) = \tau_e \wp(z) + N_{\mathrm{final},1}(z)\exp\left(-\frac{t}{\tau_e}\right) - \tau_e \wp(z)\exp\left(-\frac{t}{\tau_e}\right) \tag{28}$$

$$G_1(z) = G_{\mathrm{ref}}(z,t)\left(\frac{G_{\mathrm{final},1}(z)}{G_{\mathrm{ref}}(z)}\right)^{\exp\left(\frac{-t}{\tau_e}\right)} \tag{29}$$

where from (20) and (18)

$$N_{\mathrm{final},1}(z) = N_{\mathrm{init},1}(z) - \frac{\left(N_{\mathrm{init},1}(z) - N_0 - \frac{\alpha}{\Gamma a}\right)\left(1 - \mathcal{G}_{\mathrm{init},1}\right)}{1 - \mathcal{G}_{\mathrm{init},1} + \frac{\mathcal{G}_{\mathrm{init},1}}{G_{\mathrm{init},1}(z)}} \tag{30}$$

$$G_{\mathrm{final},1}(z) = \exp\left(-\alpha z + \Gamma a \int_0^z (N_{\mathrm{final},1}(z) - N_0)\,\mathrm{d}z\right) \tag{31}$$

$$\mathcal{G}_{\mathrm{init},1} = \exp\left(-\frac{\frac{\lambda \bar{g} E_g}{hcA}}{\frac{\int_0^L \tau_e \wp(z)\mathrm{d}z}{L} - N_0 - \frac{\alpha}{\Gamma a}}\right). \tag{32}$$

Momentarily, just before the second pulse enters SOA at $t = \tau$ from the right, the carrier density and gain are $N_{\mathrm{init},2}(z) = N_1(z,\tau)$ and $G_{\mathrm{init},2}(z) = G_1(z,\tau)$, respectively. The incidence of the second pulse depletes this recovered carrier density, giving

$$N_{\mathrm{final},2}(z) = N_{\mathrm{init},2}(z) - \frac{\left(N_{\mathrm{init},2}(z) - N_0 - \frac{\alpha}{\Gamma a}\right)\left(1 - \mathcal{G}_{\mathrm{init},2}\right)}{1 - \mathcal{G}_{\mathrm{init},2} + \frac{\mathcal{G}_{\mathrm{init},2}}{G_{\mathrm{init},2}(L-z)}} \tag{33}$$

$$G_{\mathrm{final},2}(z) = \exp\left(-\alpha z + \Gamma a \int_0^z (N_{\mathrm{final},2}(z) - N_0)\,\mathrm{d}z\right) \tag{34}$$

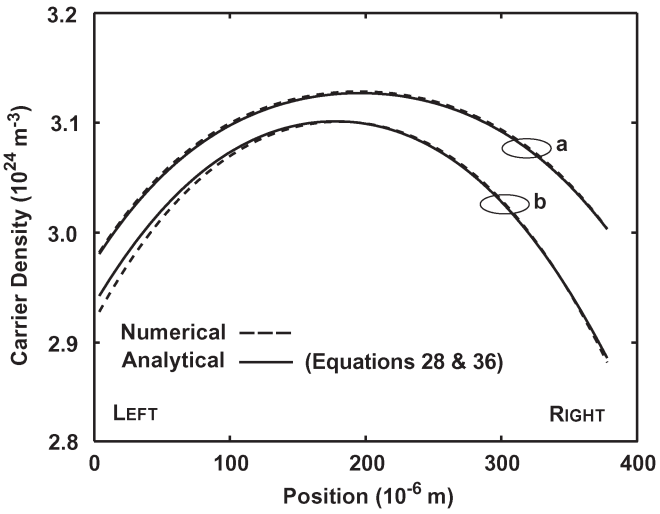

Fig. 4. Carrier density $N = \{N_1\} \cup \{N_2\}$, against position z, 100 ps after first pulse. Curve a shows the case where two counterpropagating pulses with 12.5-ps FWHM and 12.5-fJ energy are incident with a delay of 75 ps. Curve b shows two counterpropagating pulses with 5.0-ps FWHM and 25-fJ energy with a delay of 5 ps.

$$\mathcal{G}_{\mathrm{init},2} = \exp\left(-\frac{\frac{\lambda\bar{g}E_g}{hcA}}{\frac{\int_0^L N_{\mathrm{init},2}(z)\mathrm{d}z}{L} - N_0 - \frac{\alpha}{\Gamma a}}\right). \quad (35)$$

Thereafter, the carrier density and the gain replenish at a carrier-recovery rate, giving

$$N_2(z,t) = \tau_e \wp(z) + N_{\mathrm{final},2}(z)\exp\left(-\frac{t-\tau}{\tau_e}\right) - \tau_e \wp(z)\exp\left(-\frac{t-\tau}{\tau_e}\right) \quad (36)$$

$$G_2(z,t) = G_{\mathrm{ref}}(z)\left(\frac{G_{\mathrm{final},2}(z)}{G_{\mathrm{ref}}(z)}\right)^{\exp\left(\frac{-(t-\tau)}{\tau_e}\right)}. \quad (37)$$

To demonstrate the accuracy of the results derived in this section, we again use MATLAB simulations. Fig. 4 shows the carrier density $N = \{N_1\} \cup \{N_2\}$ against position z, 100 ps after the first pulse. The dashed lines (- -) show the numerical simulation results, whereas solid lines (—) show the analytical solution given by (28) and (36). It is clear from Fig. 4 that regardless of pulsewidth or the delay, expressions (28) and (36) give very good predictions of the carrier-density profiles along the SOA and its time evolution.

C. Response to Counterpropagating Identical Pulse Trains

In practice, the OPDD will be used for characterizing relative delay between pulses in counterpropagating pulse trains rather than for isolated pulses. The SOA response for pulse trains can be found by repeatedly applying the previous results for forward-propagating pulses and backward-propagating pulses. However, a much simpler result can be obtained by noting that the gain, and hence, carrier density are periodic. Suppose the gain of the SOA just before the incidence of a pulse from the left facet is G_L. Suppose τ seconds after this pulse entered from the left, an identical pulse enters from the right. Assume that the gain of the SOA is G_R, just momentarily before the incidence of the pulse from the right. Due to the periodicity of the counterpropagating pulse train, these values will be seen at T_P seconds later where T_P is the period of the pulse trains. From (17), (18), and (24), we can write the following two expressions relating G_L and G_R:

$$G_R = G_{\mathrm{ref}}\left(\frac{\frac{G_L}{G_{\mathrm{ref}}}}{G_L - (G_L-1)\mathcal{G}_{\mathrm{init}}(G_L)}\right)^{\exp\left(-\frac{\tau}{\tau_e}\right)} \quad (38)$$

$$G_L = G_{\mathrm{ref}}\left(\frac{\frac{G_R}{G_{\mathrm{ref}}}}{G_R - (G_R-1)\mathcal{G}_{\mathrm{init}}(G_R)}\right)^{\exp\left(-\frac{T_P-\tau}{\tau_e}\right)} \quad (39)$$

where G_{ref} and $\mathcal{G}_{\mathrm{init}}(G)$ are given by [cf., (18) and (25)]

$$G_{\mathrm{ref}} = \exp\left(\Gamma a\left(\tau_e\int_0^L \wp(z)\mathrm{d}z - N_0 L\right)\right) \quad (40)$$

$$\mathcal{G}_{\mathrm{init}}(G) = \exp\left(-\frac{\Gamma\lambda a E_g}{hcA} - \frac{\Gamma\lambda a E_g \alpha L}{hcA\ln(G)}\right). \quad (41)$$

Once the values for G_L and G_R are found by simultaneously solving the transcendental (38) and (39), we can calculate the time evolution of gain (and hence, the carrier-density profile) using (24) and (22). The results derived in this section will be used again in Section III-B for calculating the sensitivity of the mean voltage difference to pulse delay.

III. OPDD Performance

From the simple explanation given in Section I, it is unclear whether the proposed device will exhibit sufficient linearity, sensitivity, and speed to be useful or will be better than the photodiode design by Awad *et al.* [7].

In this section, to simplify the analysis, two identical short pulses are injected into opposite ends of the SOA, so that they counterpropagate as in Section II-B. We use the following simple model of heterostructure junction voltage V with carrier density N ignoring resistive voltage drops (which will be identical if the injection is homogeneous) [15], [17], as follows:

$$V = \eta\left(\frac{kT}{q}\right)\ln\left(\frac{N}{N_i}\right) \quad (42)$$

where η is the heterostructure ideality factor, k is Boltzmann's constant, T is the junction temperature, q is the electronic charge, and N_i is the intrinsic carrier density [18]. Using (42), and the results in Section II, we can write the following

expression for the voltage difference $\Delta V(t)$ between the end electrodes:

$$\Delta V(t) = \begin{cases} \eta \frac{kT}{q} \ln\left(\frac{N_{\text{init},1}(L)}{N_{\text{init},1}(0)}\right), & t < 0 \text{ (before first pulse)} \\ \eta \frac{kT}{q} \ln\left(\frac{N_1(L,t)}{N_1(0,t)}\right), & 0 \le t \le \tau \text{ (between pulses)} \\ \eta \frac{kT}{q} \ln\left(\frac{N_2(L,t)}{N_2(0,t)}\right), & \tau < t \text{ (after second pulse)} \end{cases} \tag{43}$$

where $N_{\text{init},1}$, N_1, and N_2 refer to the carrier densities at different stages (i.e., before first pulse, between pulses, and after second pulse) as depicted in Fig. 3. Detailed expressions for each of the above carrier-density variables at different stages of the depletion recovery process were given in Section II-B.

A. Transient Response

To derive the transient response, we consider two counterpropagating pulses with identical pulse profiles similar to the pulses considered in the previous section (refer to Fig. 3). Suppose the first pulse enters SOA from the left and after τ seconds, the second pulse enters from the right. We also assume that before the arrival of the first pulse, the SOA is in a steady state with its carrier-density and gain profiles as given in Section II-B. After rearranging the terms of $N_1(z,t)$ in (28), we get

$$N_1(z,t) = N_{\text{ss}}(z) - \Delta N_1(z) \exp\left(-\frac{t}{\tau_e}\right) \tag{44}$$

where $N_{\text{ss}}(z) = N_{\text{init},1}(z)$ and $\Delta N_1(z) = N_{\text{ss}}(z) - N_{\text{final},1}(z)$. Similarly, $N_2(z,t)$ of (36) can be written as

$$N_2(z,t) = N_{\text{ss}}(z) - \Delta N_2(z) \exp\left(-\frac{t-\tau}{\tau_e}\right) \tag{45}$$

where $\Delta N_2(z) = N_{\text{ss}}(z) - N_{\text{final},2}(z)$. Substitution of (44) and (45) to (43) and using the relation $\ln(1+x) \approx x$ for small x (i.e., $x \ll 1$) gives the time evolution of the voltage difference between the end electrodes, as follows:

$$\Delta V(t) = \begin{cases} V_{\text{ss}}, & t < 0 \\ V_{\text{ss}} - \Delta V_1 \exp\left(-\frac{t}{\tau_e}\right), & 0 \le t \le \tau \\ V_{\text{ss}} - \Delta V_2 \exp\left(-\frac{t-\tau}{\tau_e}\right), & \tau < t \end{cases} \tag{46}$$

where $V_{\text{ss}} = (\eta kT/q)\ln(N_{\text{ss}}(L)/N_{\text{ss}}(0))$, $\Delta V_1 = \eta kT \Delta N_1(L)/qN_{\text{ss}}(L)$, and $\Delta V_2 = \eta kT \Delta N_2(L)/qN_{\text{ss}}(L) - \eta kT \Delta N_2(0)/qN_{\text{ss}}(0)$. Equation (46) clearly shows that the time response is exponential decay with the time constant set by the semiconductor carrier lifetime τ_e. Note, however, that if the higher order recombination mechanisms such as Auger [19] and bimolecular recombination [19] are included in (3), this lifetime should be replaced by the differential carrier-recovery lifetime [20]–[22]. It also is interesting to note that at uniform current injection, steady-state voltage difference V_{ss} becomes zero in (46). This behavior is expected because at uniform injection, at steady state, carrier density at either end of the SOA has equal values.

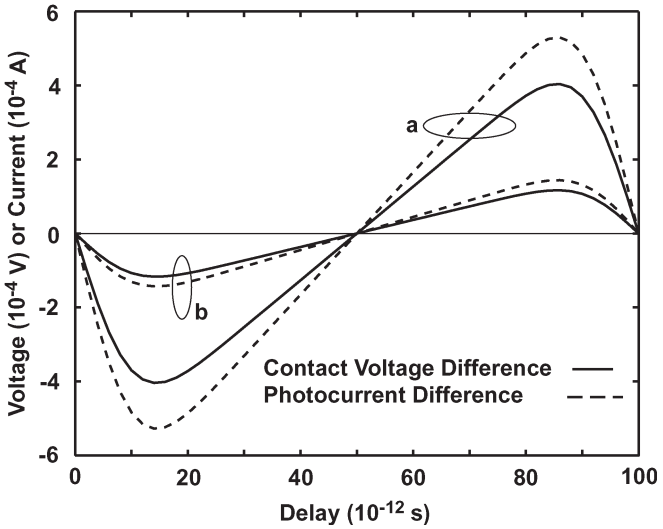

Fig. 5. Mean output (voltage or current) versus delay between the pulses for two different uniform injection rates: a) $\wp = 1.0567 \times 10^{34}\ \text{s}^{-1} \cdot \text{m}^{-3}$ and b) $\wp = 9.5768 \times 10^{33}\ \text{s}^{-1} \cdot \text{m}^{-3}$. Two counterpropagating Gaussian pulse trains with 100-ps periods and FWHM value of 12.5 ps and energy of 15.0 fJ were used.

B. Linearity

The linearity of the output versus time delay is important if the device is to be used over a wide range of delays, rather than as a part of a delay-locked loop that locks to a single value of delay. To measure the linearity, the delay of the forward pulses was swept and the mean output of the contacts and the photodiodes calculated. We used the parameters in Table I, with 10-GHz 12.5-ps FWHM 15.0-fJ Gaussian pulse trains. Fig. 5 shows the mean output versus delay between the pulses for two uniform injection rates: a) $\wp = 1.0567 \times 10^{34}\text{s}^{-1}\text{m}^{-3}$ and b) $\wp = 9.5768 \times 10^{33}\text{s}^{-1}\text{m}^{-3}$. The solid lines in Fig. 5 represent the contact voltage values, and the dashed lines represent Awad's scheme under identical conditions. The 50-ps delay corresponds to the forward pulses lying in between the backward pulses. The best linearity is obtained around this point. Both schemes show similarly good linearity. Note that for photodiodes, a responsively of 1 A/W is assumed, with perfect coupling from the SOA to the photodiodes. Use of 50% couplers would reduce this current by 50%, and coupling losses to the facet would introduce at least another 3-dB loss from the SOA to the coupler. The input signal would also be attenuated by the coupler and the facet coupling loss. Fig. 5 also shows that sensitivity of both schemes improve for high injection (and hence, high gain). This is mainly due to the extra amplification provided by the center section of the SOA. However, sensitivity improvement with gain will diminish with high input powers because, for high input powers, the center section becomes gain saturated, giving little benefit of high gain [4]. Usefully, because of the gain saturation, long center contacts give a sensitivity (volts per unit delay) independent of input power [4].

To investigate the influence of pulse energy on sensitivity (i.e., the slope of the linear section in Fig. 5), the delay of the forward pulses was swept for input pulse energies of a) 15.0 fJ and b) 30.0 fJ, and the mean output of the contacts was calculated. In both cases, we used SOA data in Table I with 10-GHz

12.5-ps Gaussian pulse trains. Fig. 5 shows the mean output voltage versus delay between the pulses for a) 15.0 fJ and b) 30.0 fJ. As expected, it shows the sensitivity increases with pulse energy.

It is useful to have a simple expression for the sensitivity (mean voltage difference per unit delay) of the contact voltage scheme in the linear region. Because spontaneous recombination is reduced, the energy of a pulse increases most if the amplifier is driven into saturation. Using (9) and (10), the energy gain can be written as [9]

$$G_E = \int_{-\infty}^{+\infty} \frac{H_{T_w}(\tau)}{E_g} \exp\left(-\alpha L + \int_0^L g(\xi,\tau)\mathrm{d}\xi\right)\mathrm{d}\tau \quad (47)$$

and after evaluating the integral using (16), we obtain

$$G_E = \frac{\ln\left(\frac{G_{\mathrm{init}}-1}{G_{\mathrm{final}}-1}\right)}{\ln\left(\frac{G_{\mathrm{init}}-1}{G_{\mathrm{final}}-1}\right) - \ln\left(\frac{G_{\mathrm{init}}}{G_{\mathrm{final}}}\right)} \quad (48)$$

where G_{init} is the SOA gain just before the arrival of the pulse, and G_{final} is the SOA gain just after the pulse exits and is given by (17). Now, for the counterpropagating periodic pulse trains considered in Section II-C, using (48), we can obtain the energy gains G_{EL} and G_{ER} for the left and right incident pulses, respectively:

$$G_{EL} = \frac{\ln\left(\frac{G_L-1}{G_{Lf}-1}\right)}{\ln\left(\frac{G_L-1}{G_{Lf}-1}\right) - \ln\left(\frac{G_L}{G_{Lf}}\right)} \quad (49)$$

$$G_{ER} = \frac{\ln\left(\frac{G_R-1}{G_{Rf}-1}\right)}{\ln\left(\frac{G_R-1}{G_{Rf}-1}\right) - \ln\left(\frac{G_R}{G_{Rf}}\right)} \quad (50)$$

where the final gains G_{Lf} and G_{Rf} can be written using (17), (38) and (39) as

$$G_{Lf} = \frac{\frac{G_L}{G_{\mathrm{ref}}}}{G_L - (G_L-1)\mathcal{G}_{\mathrm{init}}(G_L)} \quad (51)$$

$$G_{Rf} = \frac{\frac{G_R}{G_{\mathrm{ref}}}}{G_R - (G_R-1)\mathcal{G}_{\mathrm{init}}(G_R)}. \quad (52)$$

Now, consider the carrier-density change ΔN due to a pulse passing below an electrode. Using the carrier-density evolution expression (22), with input pulse shape (9), and noting the periodicity T_P of the pulse trains, we can find an approximate expression for the time evolution of ΔN (see also [15]), as follows:

$$\left.\frac{\Delta N}{N}\right|_t \approx \frac{T_P}{E_g}\delta\rho(E_g)\mathcal{T}(E_g,T_P)G_E H_{T_w}(t) \quad (53)$$

where the constants (with respect to delay τ) $\delta\rho(E_g)$ and $\mathcal{T}(E_g,T_P)$ are given by

$$\delta\rho(E_g) = \left(\frac{\wp\tau_e - N_0}{\wp\tau_e - \frac{\alpha}{\Gamma a}}\right)\exp\left(-\frac{E_g}{E_{\mathrm{sat}}}G_{E0}\right) \quad (54)$$

$$\mathcal{T}(E_g,T_P) = \frac{\tau_e E_g}{T_P E_{\mathrm{sat}}}\exp\left(-\frac{T_P}{\tau_e}\right). \quad (55)$$

The saturation energy E_{sat} is given by [9]

$$E_{\mathrm{sat}} = \frac{hcA}{\lambda\Gamma a}. \quad (56)$$

The energy gain G_{E0} of a single pulse when the SOA is initially in a steady state is given by [see (48)]

$$G_{E0} = \frac{\ln\left(\frac{G_0-1}{G_{f0}-1}\right)}{\ln\left(\frac{G_0-1}{G_{f0}-1}\right) - \ln\left(\frac{G_0}{G_{f0}}\right)} \quad (57)$$

where $G_0 = \exp(\Gamma a\tau_e\wp L - \alpha L)$ and G_{f0} given by [see (41) and (51)]

$$G_{f0} = \frac{\frac{G_0}{G_{\mathrm{ref}}}}{G_0 - (G_0-1)\mathcal{G}_{\mathrm{init}}(G_0)}. \quad (58)$$

It is interesting to note that the energy gain G_{E0} is for an SOA fed with a single optical pulse and, hence, fundamentally different from other two energy gain values G_{EL} and G_{ER} where the SOA is fed with identical counterpropagating periodic pulse trains. Applying expression (53) to each electrode and using (42), noting $\ln(1+x) \approx x$ for small x (i.e., $x \ll 1$), then time averaging (53), we write the following expression for the mean detected voltage ΔV_m:

$$\Delta V_m = \eta\frac{kT}{q}\delta\rho(E_g)\mathcal{T}(E_g,T_P)(G_{ER} - G_{EL}). \quad (59)$$

Equation (59) is a very simple expression giving the slope of the sensitivity of the mean contact voltage difference relative to delay τ. It shows that mean voltage difference is proportional to the energy gain difference of counterpropagating pulses

$$\Delta V_m \propto G_{ER} - G_{EL}. \quad (60)$$

Fig. 6 plots (59) against incident delay for SOA data given in Table I. Solid lines (—) show the curves generated by detailed calculations whereas dotted–solid lines $(-\bullet-\bullet-)$ show the results generated by (59). Fig. 7 shows the mean output voltage difference versus delay between the pulses for two different input pulse energies. The exact matches confirm the accuracy of (59).

However, it is important to look at the validity region of (59). As our main focus was to obtain an analytical expression, to reduce the complexity of the expression, and to make the

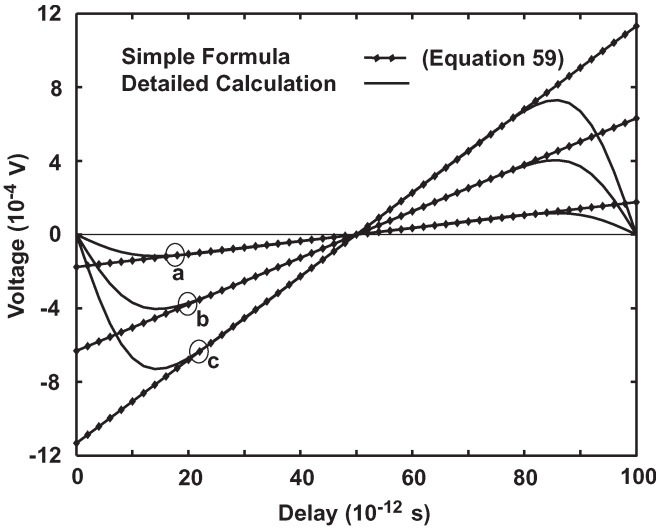

Fig. 6. Mean detected voltage difference against incident delay. Curve a is from curve b of Fig. 5, curve b is from curve a of Fig. 5, and curve c is from curve b of Fig. 7.

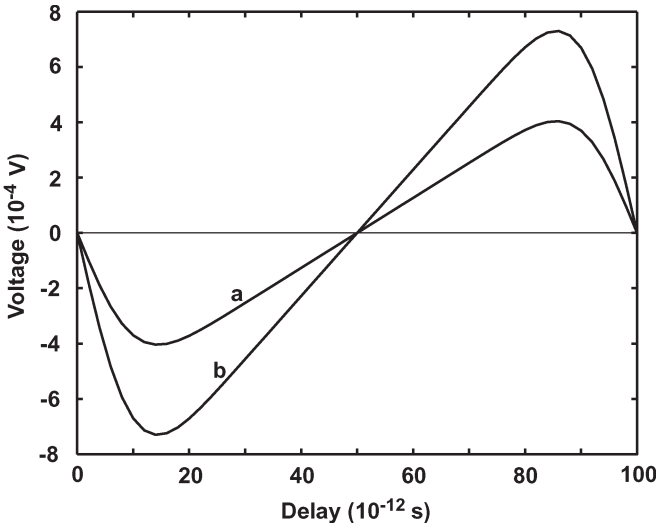

Fig. 7. Mean output voltage difference versus delay between the pulses for two different input pulse energies: a) 15.0 and b) 30.0 fJ. Two counterpropagating 10-GHz 12.5-ps Gaussian pulse trains were used.

problem tractable, we omitted some important parameters in the formulation given in (2) and (3). Some of these omitted parameters include the nonlinear gain-compression factor due to carrier heating, spectral hole burning and two-photon absorption processes [10], the Bimolecular recombination [19], and Auger processes [19]. Therefore, (59) will become inaccurate for pulses with higher energy. Fig. 8 shows the mean detected voltage difference against incident delay. Also, at higher pulse energies, the linearity seen in the femtojoule pulses seems not to hold. However, this does not limit the usability of the OPDD because input pulse energies can be regulated using external attenuators.

Also, in our analytical work, we ignore the effects of amplified spontaneous emission (ASE) noise. Therefore, it is essential to look at how this affects our analysis because ASE cannot be avoided in a real system. We used a commercially

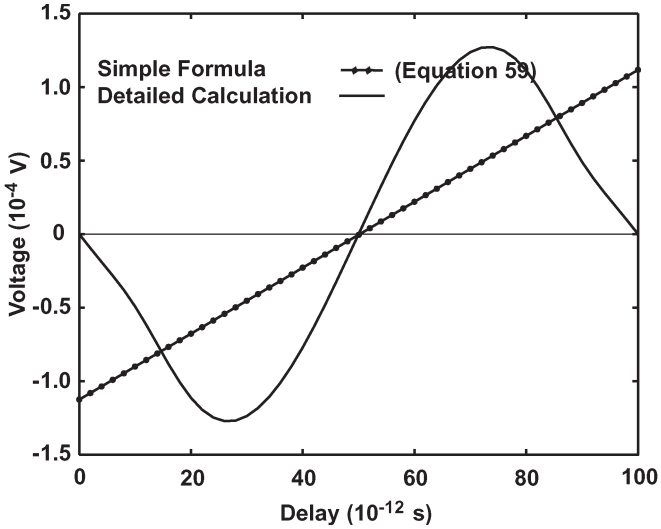

Fig. 8. Mean detected voltage difference against incident delay. Solid lines (—) show the curves generated by detailed calculations for a Gaussian pulse train with 12.5-ps FWHM and energy of 15 pJ. The dotted–solid lines $(- \bullet - \bullet -)$ show the results generated by (59) for the same pulse train. This result clearly demonstrates that the simple formula (59) fails for high-energy (around picojoule) pulses.

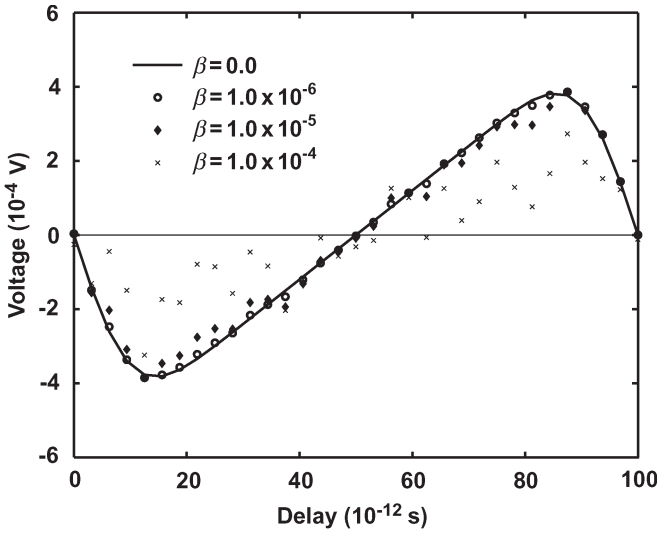

Fig. 9. Mean detected voltage difference against incident delay when ASE is present. The solid line (—) shows curve a of Fig. 5, whereas circles $(\circ)$, diamonds $(\diamond)$, and crosses $(\times)$ represent the mean differential voltage when the spontaneous-emission coupling factor is equal to $\beta = 1.0 \times 10^{-6}$, $\beta = 1.0 \times 10^{-5}$, and $\beta = 1.0 \times 10^{-4}$, respectively.

available simulator VPIcomponentMaker Active Photonics for detailed analysis including ASE noise.[1] Some details about this simulation can be found in [4]. The numerical algorithm used in the simulation program in principle is similar to [23]–[25], and hence, no further details about the implementation are given here. Fig. 9 shows the ASE impact on the differential-voltage curve a of Fig. 5. The ASE had a noise-equivalent bandwidth of 20.6 nm. The solid line (—) on Fig. 9 shows curve a of Fig. 5, whereas circles $(\circ)$, diamonds $(\diamond)$, and crosses $(\times)$ represent

[1]The authors played a key role in developing VPIcomponentMaker Active Photonics software at VPIsystems: www.vpisystems.com

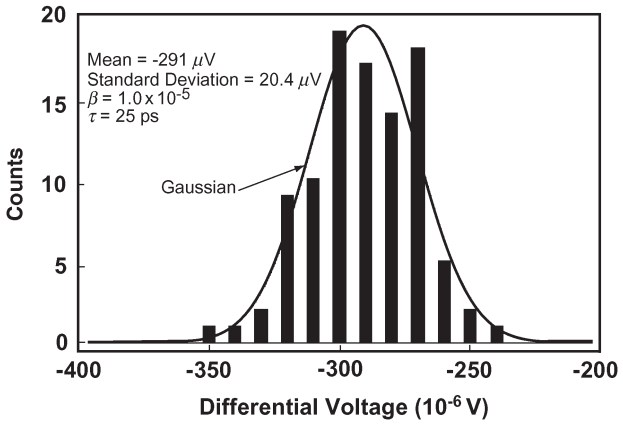

Fig. 10. Histogram (Counts against Differential Voltage) for the differential voltage for delay $\tau = 25$ ps for curve a of Fig. 5 with a spontaneous-emission coupling factor equal to $\beta = 1.0 \times 10^{-5}$.

the mean differential voltages when the spontaneous-emission coupling factor is equal to $\beta = 1.0 \times 10^{-6}$, $\beta = 1.0 \times 10^{-5}$, and $\beta = 1.0 \times 10^{-4}$, respectively. This figure clearly shows that when ASE noise is very small, our analysis provides a very good representation of the device behavior. However, if ASE noise is high (i.e., corresponding to $\beta = 1.0 \times 10^{-4}$), the sensitivity decreases, and the accuracy is reduced.

To closely look at the impact of ASE on detected differential voltage, we plotted the histogram in Fig. 10 for a pulse delay $\tau = 25$ ps for two counterpropagating identical pulse trains with 100-ps periods, 15-fJ pulse energies, and FWHMs of 12.5 ps. The solid curve in Fig. 10 shows the best fitting Gaussian with a $\text{mean} = -291.0\ \mu\text{V}$ (compared with 315.5 μV without noise, an 8% decrease) and a $\text{standard deviation} = 20.4\ \mu\text{V}$. It is clear from this figure that the effect of ASE on detected differential voltage can be approximated using a Gaussian profile and that averaging would reduce the uncertainty. The change in sensitivity could be calibrated out.

IV. Design Guidelines

The analysis in the previous section shows that increasing the sensitivity of OPDD, while having a large linear region, requires the following conditions.

- For a high sensitivity, the steady-state gain should be high, to give a large energy gain difference $G_{EL} - G_{ER}$ of (59). ASE will limit the maximum steady-state gain.
- The OPDD's response is an odd function of the delay τ and shows linear behavior around $T_P/2$. The linearity region around this point is bounded from either side by a value that is dependent on the pulsewidth. Hence, it is better to use short pulses if the range of delays is to be large.
- High pulse energies will destroy the linearity of the scheme.
- The linearity also depends on the relatively long carrier-recovery lifetime (compared with the pulse period). Therefore, the period of the pulse train must be significantly less than the carrier-recovery lifetime.
- Even though we used point electrodes at the ends to simplify the analysis, it is better to use electrodes with some length because it will reduce the contact impedance.
- The transient response of the device is exponential with a time constant set by the carrier-recovery lifetime τ_e. Therefore, the system bandwidth must be set much below this value.
- ASE will affect the sensitivity and certainty of the device response. Hence, consideration must be given to choosing an SOA with low noise performance, and the gain must kept within reasonable limits (i.e., maximum around 20 dB) for best linear performance. Averaging will reduce the uncertainty at the expense of measurement bandwidth.

V. Conclusion

We have analyzed a pulse delay discriminator utilizing a combination of cross-gain modulation, finite recovery time, and photodetection in SOAs. Unlike previous discriminator designs based on differential photodiodes [7], our optical pulse delay discriminator (OPDD), eliminates the photodiodes and two optical couplers. Therefore, the proposed method in this paper is better suited to optoelectronic integration.

We carried out a comprehensive analytical analysis of the operation of the device performance. At each stage, we demonstrated the accuracy of the derived approximate formulas for characterizing the OPDD. Analytical expressions for the transient response of OPDD were derived to demonstrate that the response is exponential with a time constant set by the carrier-recovery lifetime. We showed that it is possible to reliably measure the incident delay between counterpropagating periodic pulse trains by measuring the mean value of the induced voltage difference. Analytical and numerical evidences were provided to establish the linearity of measured mean voltage difference of contact electrodes and pulse delay.

Acknowledgment

The authors would like to thank VPIphotonics (www.vpiphotonics.com) for the use of their simulator VPIcomponentMaker Active Photonics for some of the simulations in this paper.

References

[1] S. Kawanishi and M. Saruwatari, "Ultra-high-speed PLL-type clock recovery circuit based on all-optical gain modulation in traveling-wave laser diode amplifier," *J. Lightw. Technol.*, vol. 11, no. 12, pp. 2123–2129, Dec. 1993.

[2] T. Wang, Z. Li, C. Lou, Y. Wu, and Y. Gao, "Comb-like filter preprocessing to reduce the pattern effect in the clock recovery based on SOA," *IEEE Photon Technol. Lett.*, vol. 14, no. 6, pp. 855–857, Jun. 2002.

[3] E. S. Awad, P. S. Cho, N. Moulton, and J. Goldhar, "Subharmonic optical clock recovery from 160 Gb/s using time-dependent loss saturation inside a single electroabsorption modulator," *IEEE Photon Technol. Lett.*, vol. 15, no. 12, pp. 1764–1766, Dec. 2003.

[4] A. J. Lowery and M. Premaratne, "Reduced component count optical delay discriminator using a semiconductor optical amplifier-detector," *Opt. Express*, vol. 13, no. 1, pp. 290–295, 2005.

[5] C. Bornholdt, B. Sartorius, S. Schelhase, M. Mohrle, and B. Bauer, "Self-pulsating DFB laser for all-optical clock recovery at 40 Gbit/s," *Electron. Lett.*, vol. 36, no. 4, pp. 327–328, 2000.

[6] A. D. Ellis and D. M. Spirit, "Compact 40 Gbit/s optical demultiplexer using a GaInAsP optical amplifier," *Electron. Lett.*, vol. 29, no. 24, pp. 2115–2116, 1993.
[7] E. S. Awad, C. J. K. Richardson, P. S. Cho, N. Moulton, and J. Goldhar, "Optical clock recovery using SOA for relative timing extraction between counterpropagating short picosecond pulses," *IEEE Photon. Technol. Lett.*, vol. 14, no. 3, pp. 396–398, Mar. 2002.
[8] M. Fischer, M. Dulk, E. Gamper, W. Vogt, E. Gini, H. Melchior, E. Hunziker, D. Nesset, and A. D. Ellis, "Optical 3R regenerator for 40 Gbit/s networks," *Electron. Lett.*, vol. 35, no. 23, pp. 2047–2049, 1999.
[9] G. P. Agrawal and N. A. Olsson, "Self-phase modulation and spectral broadening of optical pulses in semiconductor laser amplifiers," *IEEE J. Quantum Electron.*, vol. 25, no. 11, pp. 2297–2306, Nov. 1989.
[10] A. Mecozzi and J. Mork, "Saturation induced by picosecond pulses in semiconductor optical amplifiers," *J. Opt. Soc. Am. B*, vol. 14, no. 4, pp. 761–770, 1997.
[11] P. G. Eliseev and V. V. Luc, "Semiconductor optical amplifiers: Multifunctional possibilities, photoresponse and phase shift properties," *Pure Appl. Opt.*, vol. 4, no. 4, pp. 295–313, 1995.
[12] B. Dagens, A. Labrousse, R. Brenot, B. Lavigne, and M. Renaud, "SOA-based devices for all-optical signal processing," in *Proc. Optical Fiber Communications Conf. (OFC)*, vol. 2. Atlanta, GA, 2003, pp. 582–583.
[13] M. Premaratne, A. J. Lowery, Z. Ahmed, and D. Novak, "Modeling noise and modulation performance of fiber grating external cavity lasers," *IEEE J. Sel. Topics Quantum Electron.*, vol. 3, no. 2, pp. 290–303, Apr. 1997.
[14] A. E. Siegman, *Lasers*. Mill Valley, CA: University Science Books, 1986.
[15] R. M. Fortenberry, A. J. Lowery, and R. S. Tucker, "Up to 16 dB improvement in detected voltage using two-section semiconductor optical amplifier detector," *Electron. Lett.*, vol. 28, no. 5, pp. 474–476, 1992.
[16] A. J. Lowery, "Active photonic integrated circuits," in *Optoelectronic Devices—Advanced Simulation and Analysis*, J. Piprek, Ed. Berlin, Germany: Springer-Verlag, 2005. ISBN: 0-387-22659-1.
[17] I. Kaminow and R. S. Tucker, *Guided-Wave Optoelectronics*, T. Tamirk, Ed. New York: Springer-Verlag, 1988, ch. 5. ISBN: 0-387-22659-1.
[18] J. I. Pankove, *Optical Processes in Semiconductors*. New York: Dover, 1971.
[19] G. P. Agrawal and N. K. Dutta, *Long-Wavelength Semiconductor Lasers*. New York: Van Nostrand, 1986.
[20] T. Kallstenius, A. Landstedt, U. Smith, and P. Granestrand, "Role of nonradiative recombination in the degradation of InGaAsP/InP-based bulk lasers," *IEEE J. Quantum Electron.*, vol. 36, no. 11, pp. 1312–1322, Nov. 2000.
[21] G. E. Shtengel, D. A. Ackerman, and P. A. Morton, "True carrier lifetime measurements of semiconductor lasers," *Electron. Lett.*, vol. 31, no. 20, pp. 1747–1748, 1995.
[22] Y.-C. Chen, P. Wang, J. J. Coleman, D. P. Bour, K. K. Lee, and R. G. Waters, "Carrier recombination rates in strained-layer InGaAs–GaAs quantum wells," *IEEE J. Quantum Electron.*, vol. 27, no. 6, pp. 1451–1455, Jun. 1991.
[23] A. Sharaiha and M. Guegan, "Equivalent circuit model for multi-electrode semiconductor optical amplifiers and analysis of inline photodetection in bidirectional transmission," *J. Lightw. Technol.*, vol. 18, no. 5, pp. 700–707, May 2000.
[24] ——, "Analysis of the sign reversal of the photodetected signal response in a multielectrode semiconductor optical amplifier," *J. Lightw. Technol.*, vol. 19, no. 8, pp. 1185–1193, Aug. 2001.
[25] A. J. Lowery, "Amplified spontaneous emission in semiconductor laser amplifiers: Validity of the transmission-line laser model," *Proc. Inst. Elect. Eng., J Optoelectron.*, vol. 137, no. 4, pp. 241–247, 1990.

Malin Premaratne (S'95–M'98–SM'03) received the B.Sc. (maths.), B.E. (elec.) with first-class honors from the University of Melbourne, Melbourne, Australia, in 1995, and the Ph.D. degree from the same University in 1998.

From 1998 to 2000, he was with the Photonics Research Laboratory, a division of the Australian Photonics Cooperative Research Centre (APCRC), the University of Melbourne, where he was the Coproject Leader of the APCRC Optical Amplifier Project. During this period, he worked with Telstra, Australia, and Hewlett Packard, USA through the University of Melbourne. From 2000 to 2003, he was involved with several leading startups in the photonic area either as an employee or a consultant. During this period, he had also served in the editorial boards of SPIE/Kluwer and Wiley publishers in the optical communications area. From 2001 to 2003, he worked as the Product Manager (Research and Development) of VPIsystems Optical Systems group. Since 2000, he has been appointed as a Senior Associate/Senior Fellow of the University of Melbourne. Since 2003, he has led the research program in high-performance computing applications to complex system simulations at the Advanced Computing and Simulation Laboratory (AXL) at Monash University, Australia. He has published over 75 research papers in the areas of semiconductor lasers, EDFA and Raman amplifiers, optical network-design algorithms, and numerical-simulation techniques. His current research interests include the areas of optical network design, analysis, and configuration methods; simulation of optical and electromagnetic interaction with biological and other turbid substances; grid and cluster computing; and realistic scene rendering in computer graphics using optical-physics-based methods.

Dr. Premaratne served as the Chairman of IEEE Lasers and Electro-Optics Society in Victoria, Australia, in 2001.

Arthur James Lowery (M'92–SM'96) was born in Yorkshire, U.K., in 1961. He received the B.Sc. degree (first-class hons.) in applied physics from the University of Durham, U.K., in 1983 and the Ph.D. degree in electrical and electronic engineering from the University of Nottingham, Nottingham, U.K., in 1988.

From 1983 to 1984, he worked at Marconi Radar Systems Ltd., U.K. In 1984, he joined the University of Nottingham as a Lecturer and pioneered time-domain field modeling of semiconductor lasers known as the transmission-line laser model. In 1990, he immigrated to Australia to become a Senior Lecturer in the newly formed Photonics Research Laboratory at the University of Melbourne. After working on photonic-CAD, packet switching, and laser ranging, he was promoted to Associate Professor and Reader in 1993. He continued to develop novel time-domain simulation techniques and to lead collaborative research as a Fellow of the Australian Photonics Cooperative Research Centre. In 1996, he cofounded Virtual Photonics Pty. Ltd. with P. Gurney. Virtual Photonics merged with BNeD, Berlin, in 1998, with him as Chief Technology Officer, leading the development of VPI's physical-level photonic design automation tools such as VPItransmissionMaker and VPIcomponentMaker, which are widely used in the industry and academia for development, research, and teaching. In 2004, he was appointed Professor of Electrical and Computer Systems Engineering at Monash University, Melbourne, Australia, where he is working on active photonic circuits and the applications of photonic technology. He has published more than 170 papers and four book chapters on the simulation of photonic devices and circuits and photonic applications such as mode locking, packet switching, transmission systems, and high-speed circuits.

He is a Fellow of the Institution of Electrical Engineers (IEE), U.K.